



## Article

# Study on the Accuracy of Fracture Criteria in Predicting Fracture Characteristics of Granite with Different Occurrence Depths

Chenbo Liu <sup>1</sup>, Gan Feng <sup>1,2,\*</sup>, Hongqiang Xie <sup>1,\*</sup>, Jilan Wang <sup>1</sup>, Zhipan Duan <sup>1</sup>, Ye Tao <sup>1</sup>, Gongda Lu <sup>1</sup>, Huining Xu <sup>1</sup>, Yaoqing Hu <sup>3</sup>, Chun Li <sup>3</sup>, Yuefei Hu <sup>3</sup>, QiuHong Wu <sup>4</sup> and Lu Chen <sup>5</sup>

<sup>1</sup> College of Water Resource & Hydropower, Sichuan University, Chengdu 610065, China

<sup>2</sup> Ministry of Education, Key Laboratory of Deep Earth Science and Engineering, Sichuan University, Chengdu 610065, China

<sup>3</sup> College of Mining Engineering, Taiyuan University of Technology, Taiyuan 030024, China

<sup>4</sup> Work Safety Key Lab on Prevention and Control of Gas and Roof Disasters for Southern Coal Mines, Hunan University of Science and Technology, Xiangtan 411201, China

<sup>5</sup> School of Civil Engineering, Changsha University of Science & Technology, Changsha 410000, China

\* Correspondence: fenggan@whu.edu.cn (G.F.); alex\_xhq@scu.edu.cn (H.X.);

Tel.: +86-135-0971-7523 (G.F.); +86-172-0828-1067 (H.X.)

**Abstract:** The fracture network of a deep geothermal reservoir forms the place for heat exchange between injected fluid and rock mass with high temperature. The fracture resistance ability of reservoir rocks will affect the formation of fracture-network structure, heat exchange and transmission characteristics, and reservoir mechanical stability. However, there are few reports on the fracture toughness and trajectory prediction of geothermal reservoirs with different depths. In this paper, the modified maximum tangential stress criterion (MMTS) is analyzed. The results show that the experimental data are significantly different from the theoretical estimate of MMTS under the influence of different occurrence depths. It is found that the fracture process zone (FPZ) seriously affects the accuracy of predicting fracture initiation angle and mixed-mode (I+II) fracture toughness by MMTS. The FPZ value, considering the influence of different occurrence depths, is modified, and the accuracy of MMTS in predicting the fracture mechanical characteristics of granite is improved. In addition, the mechanical test results show that the Brazilian splitting strength ( $\sigma_t$ ) of granite fluctuates increase with the increase in temperature. With the increase in deviatoric stress, the Brazilian splitting strength and the Brazilian splitting modulus of rock show a trend of first increasing, then decreasing, and then increasing.

**Keywords:** rock mechanical properties; MMTS; geothermal development; geothermal reservoir; different depth of occurrence



**Citation:** Liu, C.; Feng, G.; Xie, H.; Wang, J.; Duan, Z.; Tao, Y.; Lu, G.; Xu, H.; Hu, Y.; Li, C.; et al. Study on the Accuracy of Fracture Criteria in Predicting Fracture Characteristics of Granite with Different Occurrence Depths. *Energies* **2022**, *15*, 9248. <https://doi.org/10.3390/en15239248>

Academic Editor: José António Correia

Received: 22 October 2022

Accepted: 4 December 2022

Published: 6 December 2022

**Publisher's Note:** MDPI stays neutral with regard to jurisdictional claims in published maps and institutional affiliations.



**Copyright:** © 2022 by the authors. Licensee MDPI, Basel, Switzerland. This article is an open access article distributed under the terms and conditions of the Creative Commons Attribution (CC BY) license (<https://creativecommons.org/licenses/by/4.0/>).

## 1. Introduction

Geothermal energy has the advantages of being clean and renewable, having wide distribution and high heat storage, and is regarded as a renewable energy with great potential [1–4]. It can be used for power generation, heating, planting, breeding, and so on [5]. According to the heat storage temperature and burial depth, it can be divided into shallow geothermal resources and deep geothermal resources [6–8]. According to theoretical estimates, the total amount of geothermal energy stored within the upper 10 km of the Earth's crust is about  $1.3 \times 10^{27}$  J, which can be used for approximately 21.7 million years globally [9,10]. Deep geothermal resources are stored in hot dry rock. The hot dry rock mass is compact and has very little permeability. Traditional geothermal extraction methods are difficult to exploit effectively, so it is necessary to build an enhanced geothermal system (EGS). In recent years, the construction of EGS projects has been carried out. According to statistics, by the end of 2021, 41 EGS projects had been built across the world [11], such as the Fenton Hill Project in the United States [12], the Rosemanowes project in

Britain [13], the Mauerstetten project in Germany [14], and the Soultz project in France [15]. Among them, the most successful project is the Soultz project in France, which has a power generation capacity of megawatts [15]. The ability of the hot dry rock reservoir to resist fracture damage directly affects its fracture-network structure, heat transfer characteristics, and reservoir mechanical stability. Therefore, it is necessary to study the failure fracture mechanical properties of geothermal reservoirs. However, due to the complex geological environment of geothermal reservoirs and the different occurrence depths of reservoirs, there is a lack of research on the fracture mechanics behavior of geothermal reservoirs.

The fracture toughness of rock is an important element in fracture mechanics and reflects the ability of material to resist crack propagation. Previous studies have shown that modified maximum tangential stress (MMTS) theory is suitable for the fracture mechanics of brittle materials such as rocks, and it is commonly used to predict the fracture toughness and crack initiation angle of rocks. Ayatollahi et al. [16] compared the predicted value of fracture toughness ratio ( $K_{IIC}/K_{IC}$ ) with the experimental value using the MTS criterion considering stress singularity,  $T$ -stress, and the second non-singular term, and the results showed that the predicted value was in good agreement with the experimental value. Akbardoost et al. [17] predicted the fracture resistance of samples with different geometric forms by MMTS criterion considering stress non-singular terms ( $T$ -stress,  $A_3$ , and  $B_3$ ); the obtained results were in good agreement with the experimental values, and  $A_3$  could be used to accurately calculate the length of the fracture process zone (FPZ). Yang et al. [18] studied the influence of water damage on the mechanical properties of rock fracture and found that the MMTS criterion was consistent with the test results when the damage degree was low, but it was inconsistent with the test results when the damage degree was deepened. Wang et al. [19] modified the GMTS criterion by considering parallel and vertical non-singular terms ( $T_x$  and  $T_y$ ), and conducted numerical simulation based on the discontinuous deformation analysis (DDA) procedure. It was found that the simulation results were in good agreement with the test results, which verifies the accuracy of the modified GMTS criterion. Aliha et al. [20] studied the effect of loading rate on the composite (I+II) fracture behavior of short bend beam specimens and compared the prediction results of MMTS criterion with experimental results, showing that MMTS has a good accuracy in predicting fracture toughness. The radius of crack propagation plays an important role in predicting fracture behavior. Feng et al. [21,22] carried out different times of thermal cycle tests on granite at 20~300 °C and concluded that there was an error between the prediction results of MMTS and the results obtained by experimental back-calculation. Tang et al. [23–25] found in their study that the modified MTS criterion after introducing  $T$ -stress could capture the crack growth path more accurately; the growth path presented smooth characteristics, and the tensile fracture was enhanced with the increase in cohesion or the decrease in tensile strength.

The rock environment in underground engineering is very complex. Generally speaking, from the surface to the interior of the earth, the temperature rises by 20 °C to 30 °C for every 1 km of depth [26]. The development and operation process of geothermal reservoirs involves the complex spatio-temporal evolution law of temperature field, stress field, and hydrodynamic field in fractured rock mass [27–29]. Due to the different occurrence depths, the temperature and stress environment of geothermal reservoirs are different. In order to obtain more heat during geothermal extraction, geothermal reservoirs often require a sufficient fracture-network structure to provide more area for heat exchange. On the other hand, when reservoir fractures develop to a certain extent, uncontrolled fractures will cause damage to the surrounding strata, resulting in massive loss of injected fluids, engineering earthquakes, and other problems. Therefore, it is of great significance to deeply understand how different occurrence depths affect the fracture mechanical properties of geothermal reservoirs. Some scholars have studied the physical and mechanical properties of rocks at different occurrence depths. Zhang et al. [30] studied the AE sequence characteristics of coal in different damage and failure processes, and the research showed that the AE signal intensity of coal in the temperature pressure coupling process was higher than that under

uniaxial compression and heating. Zhang et al. [31] found that the use of multi-source data and an integrated model will significantly improve the accuracy of wellbore instability and leakage prediction in high-pressure, high-temperature (HPHT) gas fields. Wang et al. [32] studied the properties of Jinping marble, Bayu granite, and Longchang sandstone under the coupling conditions of HPHT. The results show that the peak strength, elastic modulus, and fracture mode of rock vary with the change of rock type and temperature. Guo et al. [33] established a thermo-hydro-mechanical-damage (THMD) model to study the evolution of multiple physical fields during HDR hydraulic fracturing. Kumari et al. [34] carried out hydraulic fracturing tests on rocks under a confining pressure of 0~60 MPa and a temperature of ~300 °C. The study showed that the reservoir failure pressure increased linearly with the increase in confining pressure and decreased linearly with the increase in temperature. Meng et al. [35] conducted triaxial cyclic loading and unloading tests on rock specimens treated with different temperatures. The study showed that the increase in temperature could significantly degrade the physical properties of rock, and the increase in confining pressure could improve the strength and deformation of rock. Ding et al. [36] conducted a CO<sub>2</sub> seepage test on sandstone under the action of thermodynamic coupling, and the study showed that the permeability of sandstone decreased with the rise in stress, and first decreased and then increased with the increase in temperature.

It can be seen that, with its accuracy, MMTS can be used to predict the fracture characteristics of rock. However, how accurate is MMTS rock prediction considering the influence of different occurrence depths of geothermal reservoirs? Further research is needed. Meanwhile, there is a lack of research considering the failure and fracture mechanical behavior of reservoir rocks under the influence of geothermal reservoir depth. In fact, complex physical and chemical reactions occur in rock at different occurrence depths (temperature and three-dimensional stress environment), which affect the structure and properties of rock and inevitably affect the fracture process zone (FPZ) at rock fracture tips. Therefore, when MMTS is used to predict rock fracture characteristics, the influence of thermo-mechanical coupling on rock physical and mechanical properties should be considered.

Therefore, in this paper, the modified maximum tangential stress (MMTS) criterion is first analyzed in this study. The granite samples were then subjected to heat treatment under different temperatures and pressures, and the fracture toughness and tensile strength were tested. Finally, the prediction results of MMTS are compared with the experimental results, and the variation of the critical crack propagation radius ( $r_c$ ) with temperature and three-dimensional stress is analyzed. The accuracy of MMTS in predicting the fracture characteristics of geothermal reservoir rocks considering the influence of different occurrence depths is revealed.

## 2. The Modified Maximum Tangential Stress (MMTS) Criterion

According to the MTS criterion proposed by Erdogan and Sih, when the shear stress,  $\sigma_\theta$ , is equal to the tensile strength of the material, a crack is formed along the maximum tangential stress ( $\theta_0$ ) from the crack tip [37]. Mirsayar et al. [38] pointed out that considering the influence of higher-order terms higher than  $T$ -stress in practical engineering applications would increase the difficulty of solving the problem, so only the role of  $T$ -stress should be studied in higher-order terms. Therefore, according to the Williams infinite series expansion [39], not only the effect of the singular term of stress component, namely stress intensity factor, but also the effect of the non-singular constant term  $T$ -stress on crack propagation were considered, so the tangential stress component at the crack tip could be expressed as follows:

$$\sigma_\theta = \frac{1}{\sqrt{2\pi r}} \cos^2 \frac{\theta}{2} \left( K_I \cos \frac{\theta}{2} - 3K_{II} \sin \frac{\theta}{2} \right) + T \sin^2 \theta \quad (1)$$

where  $\theta$  and  $r$  are the traditional crack tip coordinates, as shown in Figure 1,  $K_I$  and  $K_{II}$  are Mode I and Mode II stress intensity factors, respectively, and  $T$  is  $T$ -stress, which is independent of the distance to the crack tip [40].

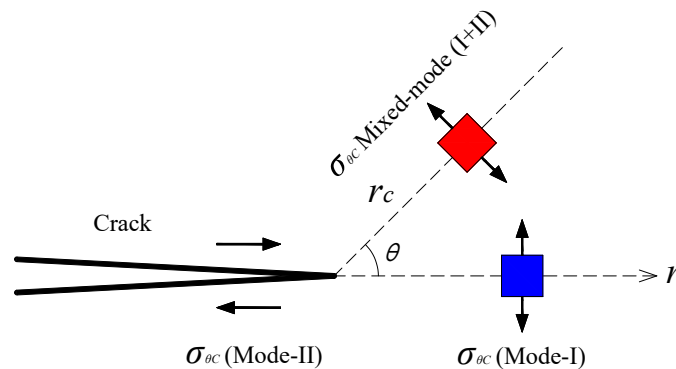


Figure 1. The maximum tangential stress (MTS) criterion [41,42].

The calculation formula of  $T$ -stress is as follows [43]:

$$T = \frac{P}{2RB} T^* \left( \frac{a}{R}, \frac{S}{D}, \alpha \right) \quad (2)$$

where  $T^*$  is a dimensionless geometric parameter, which is related to fracture length ratio, span ratio, and fracture inclination angle [21,22]. By differentiating  $\sigma_\theta$  with respect to  $\theta$ , the crack initiation angle,  $\theta_0$ , of mixed-mode (I+II) type can be obtained. The formula is as follows:

$$\frac{\partial \sigma_\theta}{\partial \theta} = 0, [K_I \sin \theta_0 + K_{II}(3 \cos \theta_0 - 1)] - \frac{16T}{3} \sqrt{2\pi r_c} \cos \theta_0 \sin \frac{\theta_0}{2} = 0 \quad (3)$$

where  $r_c$  is the length of the fracture process zone (FPZ), which is regarded as an inherent characteristic of the material and has nothing to do with the shape of the sample, loading conditions and mixing mode [44];  $r_c$  indicates that the fracture process zone has been damaged and cannot bear any load [38]. Schmidt proposed an equation based on the maximum normal stress theory to calculate  $r_c$  [45]:

$$r_c = \frac{1}{2\pi} \left( \frac{K_{IC}}{\sigma_t} \right)^2 \quad (4)$$

where  $K_{IC}$  is pure Mode I fracture toughness and  $\sigma_t$  is tensile strength, which can be calculated by Brazilian splitting experiment;  $r_c$  can be obtained from Equation (4) and  $\theta_0$  can be obtained by substituting it into Equation (3). Substituting  $r_c$  and  $\theta_0$  into Equation (1), the calculation formula of critical tangential stress,  $\sigma_{\theta c}$ , under mixed-mode (I+II) type can be obtained, which can be used to predict the fracture of mixed-mode (I+II) type brittle materials or quasi-brittle materials. The calculation formula is as follows:

$$\sigma_{\theta\theta} \sqrt{2\pi r_c} = \cos^2 \frac{\theta_0}{2} \left( K_I \cos \frac{\theta_0}{2} - 3K_{II} \sin \frac{\theta_0}{2} \right) + \sqrt{2\pi r_c} T \sin^2 \theta_0 \quad (5)$$

When pure Mode I fracture occurs,  $\theta_0 = 0$ , which satisfies:

$$K_{IC} = \sigma_{\theta\theta} \sqrt{2\pi r_c} \quad (6)$$

Based on Equations (5) and (6), the relationship between mixed-mode (I+II) fracture toughness,  $K_I$  and  $K_{II}$ , and pure Mode I fracture toughness,  $K_{IC}$ , can be established as follows:

$$K_{IC} = \cos^2 \frac{\theta_0}{2} \left( K_I \cos \frac{\theta_0}{2} - 3K_{II} \sin \frac{\theta_0}{2} \right) + \sqrt{2\pi r_c} T \sin^2 \theta_0 \quad (7)$$

The effective stress intensity factor can be calculated as follows:

$$K_{eff} = \sqrt{K_I^2 + K_{II}^2} \quad (8)$$

The effective fracture toughness and pure Mode I fracture toughness ratio,  $K_{eff}/K_{IC}$ , can be obtained from Equations (7) and (8), and its theoretical expression is as follows [18]:

$$\frac{K_{eff}}{K_{IC}} = \sqrt{Y_I^2 + Y_{II}^2} \left[ \cos^2 \frac{\theta_0}{2} \left( Y_I \cos \frac{\theta_0}{2} - 3Y_{II} \sin \frac{\theta_0}{2} \right) + T * \sqrt{\frac{2\pi r_c}{a}} \sin^2 \theta_0 \right]^{-1} \quad (9)$$

where  $Y_I$  is the normalized Mode I stress intensity factor and  $Y_{II}$  is the normalized Mode II stress intensity factor. The fracture toughness can be expressed by the mixed-mode parameter,  $M^e$ , whose theoretical expression is as follows [21,22]:

$$M^e = \frac{2}{\pi} \tan^{-1} \frac{K_I}{K_{II}} \quad (10)$$

where the value of  $M^e$  ranges from 0 to 1. When the pure Mode I fracture occurs, the value of  $M^e$  is 1. When the pure Mode II fracture occurs, the  $M^e$  value is 0. While mixed-mode (I+II) fracture occurs, the value of  $M^e$  is related to the fracture dip angle.

Under the action of external load, stress concentration occurs at the fracture tip. The initiation, propagation, interaction, and aggregation of internal microcracks are crucial reasons for the instability and failure of rock. The stress condition is affected by irregular crystal structure, original pores and cracks, friction force, and other factors [46], which will lead to high shear and tensile stress at the fracture tip. When stress exceeds the strength of molecular and atomic bonds, chemical bonds break and microcracks form [47]. Before reaching the peak load, microcracks constantly sprout at the crack tip, and these microcracks nucleate and propagate to form the microcrack expansion area, namely the fracture process zone (FPZ) of rock [18]. When the peak load is reached, the crack tip begins to crack and expands, finally forming macroscopic cracks.

FPZ is an important fracture mechanical parameter of rocks. Its size is closely related to the size of specimens and the properties of rocks, such as fracture toughness, fracture trajectory, and fracture energy [47].  $r_c$  can be regarded as the length of FPZ. When  $r_c$  is changed, it can be seen from Equation (3) that the fracture initiation angle,  $\theta_0$ , of rock is changed, and from Equation (9) that the predicted value of mixed-mode (I+II) fracture toughness is changed. In conclusion, FPZ seriously affects fracture initiation angle and mixed-mode (I+II) fracture toughness, which further affects the accuracy of MMTS in predicting rock fracture behavior. If the value of crack growth radius,  $r_c$ , can be known, the characteristics such as crack growth angle, fracture toughness value, and fracture trajectory can be predicted by MMTS criterion.

### 3. Methodology

In order to draw the fracture envelope of MMTS, it can be seen from Equations (4), (9), and (10) that the values of tensile strength and the Mode I, Mode II, and mixed-mode (I+II) fracture toughness of rock should be tested. Therefore, in this section, we first introduce the rock samples used in this experiment. We will then introduce the thermal and mechanical experiments, and finally, we will introduce the mechanical experiments.

The granite samples selected in this paper were taken from Miluo, Hunan Province. Through X-ray diffraction and thin section identification, the granite samples used in this experiment are mainly composed of quartz, plagioclase, alkaline feldspar, biotite, and Muscovite [48].

The geothermal reservoir is located in different temperature and three-dimensional stress in situ stress environments at various occurrence depths. The samples are set under different temperature and three-dimensional pressure conditions for heat treatment. Six groups of experimental conditions were set: the first group was set as axial pressure of 25 MPa, lateral pressure of 20 MPa, and temperature of 100 °C. In the second group, the axial pressure was 40 MPa, the lateral pressure was 30 MPa, the temperature was 130 °C. In the third group, the axial pressure was 50 MPa, the lateral pressure was 35 MPa, and



temperature was 100 °C. In the fourth set, the axial pressure was 50 MPa, the lateral pressure was 40 MPa, and the temperature was 150 °C. In the fifth set, the axial pressure was 60 MPa, the lateral pressure was 40 MPa, and the temperature was 100 °C. In the sixth set, the axial pressure was 75 MPa, the lateral pressure was 50 MPa, and the temperature was 200 °C. Heat treatment experiments of granite were carried out using the multifunctional high temperature rock triaxial servo control permeation testing machine of Taiyuan University of Technology. During the test, the cylinder sample was first placed into the heating furnace, and the pressure was applied to the set value at the axial loading rate of 0.5 kN/s and the lateral loading rate of 0.02 mm/min, and it was then heated at the heating rate of 5 °C/min. When the set temperature was reached, the heat was held for two hours, and then the heating was stopped and the pressure was reduced. The sample was allowed to cool naturally to room temperature [48].

The granite samples after the heat treatment tests were processed by wire cutting into standard Brazilian disc and standard semi-circular bend (SCB) samples, which were used for tensile strength tests and fracture toughness tests, respectively. Using the International Society for Rock Mechanics (ISRM)-recommended standard SCB sample geometry size range [49], the sample processing parameters can be determined. In this experiment, the diameter ( $D$ ) of the sample is 50 mm, the thickness ( $B$ ) is 20 mm, the length of the artificial groove ( $a$ ) is 12.5 mm, and the span of the support ( $S$ ) is 30.5 mm. Various loading modes can be obtained by changing the angle ( $\alpha$ ) between the pre-cut notch and the loading direction. When  $\alpha = 0^\circ$ , it belongs to Mode I fracture. When  $\alpha = 54^\circ$ , it belongs to Mode II fracture. In this study,  $\alpha = 30^\circ$  were selected as the mixed-mode (I+II) fracture mode.

The three point bending fracture mechanics test was then carried out on the SCB samples. An INSTRON 5967 testing machine of Sichuan University was used to test the fracture toughness of the SCB samples under mechanical loading. During the test, the displacement-controlled loading mode was adopted, and the loading rate was 0.002 mm/s. At the same time, the rock mechanics test system MTS815 Flex Test GT model of Sichuan University was used to test the tensile strength of the Brazilian disc samples after heat treatment. The loading rate was 0.1 mm/min. The experimental process is shown in Figure 2.

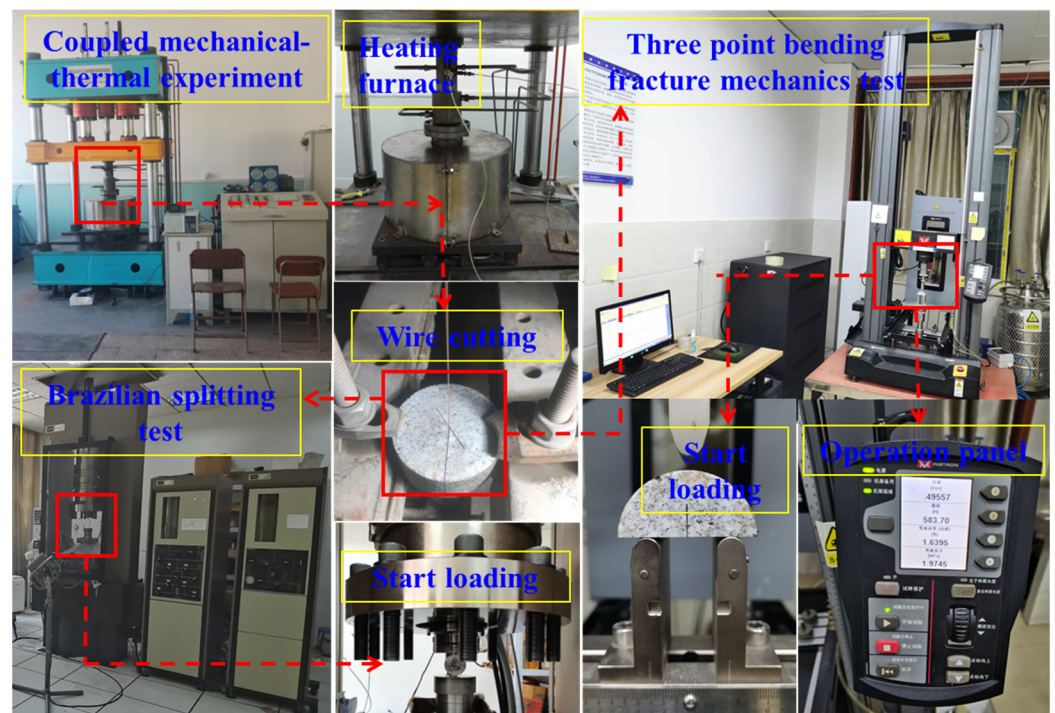


Figure 2. Test flow chart (Some pictures were modified from reference [48]).

## 4. Experimental Results

In Section 3, the experimental results of the fracture toughness and tensile strength of granite specimens affected by different thermal and force treatment conditions are obtained after the thermal-mechanical treatment test, three-point bending fracture mechanics test, and Brazil splitting test.

### 4.1. Test Results of Fracture Toughness

In Section 3, the thermal-mechanical treatment test and three-point bending fracture mechanics test were carried out on granite specimens. The average value of the obtained experimental results is shown in Table 1.

**Table 1.** Average values of the effective fracture toughness of granite.

Group Number	Conditions of Experiment	Fracture Mode	$K_{eff}$ (MPa·m <sup>1/2</sup> )
Group 1	The axial pressure is 25 MPa, the lateral pressure is 20 MPa, and the temperature is 100 °C	Mode I	1.396
		Mixed mode (I+II) ( $\alpha = 30^\circ$ )	1.086
Group 2	The axial pressure is 40 MPa, the lateral pressure is 30 MPa, and the temperature is 130 °C	Mode II	0.437
		Mode I	1.344
Group 3	The axial pressure is 50 MPa, the lateral pressure is 35 MPa, and the temperature is 100 °C	Mixed mode (I+II) ( $\alpha = 30^\circ$ )	1.137
		Mode II	0.532
Group 4	The axial pressure is 50 MPa, the lateral pressure is 40 MPa, and the temperature is 150 °C	Mode I	1.536
		Mixed mode (I+II) ( $\alpha = 30^\circ$ )	0.915
Group 5	The axial pressure is 60 MPa, the lateral pressure is 40 MPa, and the temperature is 100 °C	Mode II	0.416
		Mode I	1.481
Group 6	The axial pressure is 75 MPa, the lateral pressure is 50 MPa, and the temperature is 200 °C	Mixed mode (I+II) ( $\alpha = 30^\circ$ )	0.949
		Mode II	0.407
Group 5	The axial pressure is 60 MPa, the lateral pressure is 40 MPa, and the temperature is 100 °C	Mode I	1.581
		Mixed mode (I+II) ( $\alpha = 30^\circ$ )	0.969
Group 6	The axial pressure is 75 MPa, the lateral pressure is 50 MPa, and the temperature is 200 °C	Mode II	0.381
		Mode I	1.357
Group 6	The axial pressure is 75 MPa, the lateral pressure is 50 MPa, and the temperature is 200 °C	Mixed mode (I+II) ( $\alpha = 30^\circ$ )	0.925
		Mode II	0.461

### 4.2. Brazilian Disk Splitting Experiment Results

In Section 3, the thermo-mechanical treatment test and the Brazilian disk splitting mechanics test were carried out on granite specimens. After data processing, the tensile strength results of granite under different thermo-mechanical treatment conditions were obtained. Concurrently, the Brazilian disk splitting test is often a conventional experimental method to study the mechanical properties of rocks. Therefore, the tensile strength and the Brazilian splitting modulus obtained from the Brazilian splitting experiment were studied. These were used to explore the influence of different occurrence depths on the mechanical properties of granite reservoirs.

#### 4.2.1. Tensile Strength

The tensile strength of granite under different temperature and three-dimensional stress is shown in Figure 3.

According to Figure 3a, the Brazilian splitting strength,  $\sigma_t$ , of granite fluctuates with the increase in temperature. The Brazilian splitting strength at 150 °C reaches the maximum value (9.451 MPa), which is 28% higher than that of the untreated sample. According to Figure 3b, with the increase in deviatoric stress, the Brazilian splitting strength first increases, then decreases, and then increases. When the deviatoric stress is 5 MPa, the Brazilian splitting strength reaches the maximum value (9.122 MPa) and then decreases gradually with the increase in the deviatoric stress. When the deviatoric stress increases to 20 MPa, the Brazilian splitting strength of granite decreases to the minimum value (5.824 MPa), which is 21% lower than that of the untreated sample. When the deviatoric stress is 10 MPa, the Brazilian splitting strength of granite is 7.873 MPa at 130 °C and 9.451 MPa at 150 °C, increasing by 20%. When the temperature is 100 °C, the Brazilian splitting strength of granite is 9.122 MPa when the deviatoric stress is 5 MPa and 5.824 MPa

when the deviatoric stress is 20 MPa, decreasing by 36%. Therefore, with the change of external temperature and pressure, the Brazilian splitting strength of granite will not continue to decrease, but will increase.

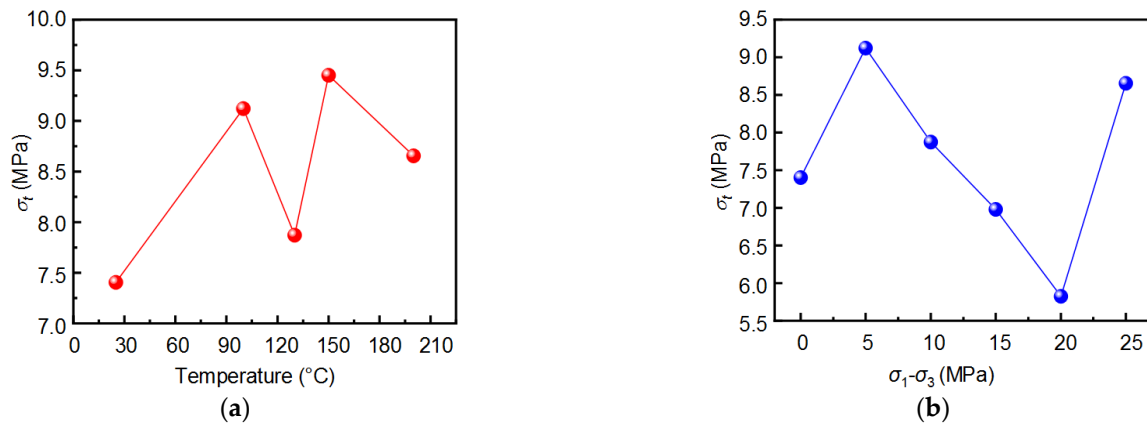


**Figure 3.** Brazilian splitting strength curves under different heat treatment conditions. (a) Brazilian splitting strength curve with temperature; (b) Brazilian splitting strength curve with deviatoric stress.

#### 4.2.2. Brazilian Splitting Modulus

The ability of rock to resist elastic deformation and failure can be determined by the Brazilian splitting experiment. Brazilian splitting modulus ( $E_T$ ) was used as the benchmark for judgment. The specific method is as follows: divide the ordinate of the load-displacement curve by the area of the meridional plane of the rock and the abscate by the diameter of the specimen to obtain the slope of the elastic phase, namely the Brazilian splitting modulus ( $E_T$ ) [50]. The Brazilian splitting modulus curve of the sample was thus drawn, as shown in Figure 4:

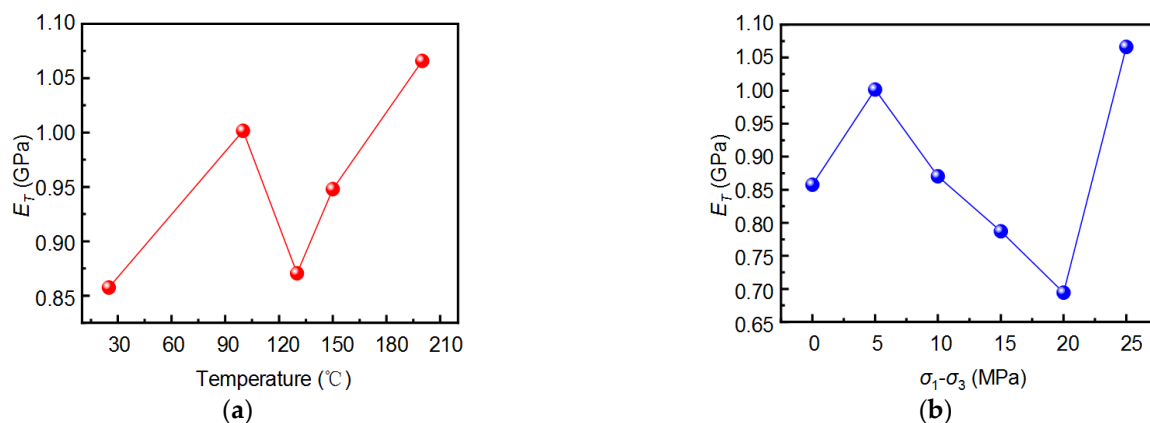


**Figure 4.** Variation curve of Brazilian splitting modulus of granite. (a) Brazilian splitting modulus variation curve with temperature; (b) Brazilian splitting modulus variation curve with deviatoric stress.

As can be seen from Figure 4a, with the temperature increasing, the Brazilian splitting modulus ( $E_T$ ) first increases, then decreases, and then increases, which is generally higher than the Brazilian splitting modulus at room temperature. When the Brazilian splitting modulus ( $E_T$ ) reaches its maximum value (1.07 GPa) at 200  $^{\circ}\text{C}$ , which is 24% higher than that at room temperature, the rock has the strongest ability to resist elastic deformation and failure. Pressure compacts the pores and cracks inside the rock, offsets the deterioration of rock properties caused by temperature, and improves the mechanical properties of the rock. As can be seen from Figure 4b, with the increase in deviatoric stress, the Brazilian splitting modulus generally shows an upward-down-upward trend, which is consistent with the variation trend of Brazilian splitting strength with the escalation of deviatoric stress. When



the deviatoric stress is 20 MPa, the Brazilian splitting modulus reaches the minimum value (0.69 GPa), which decreases by 19% compared with the room temperature condition, indicating that the thermal damage inside the rock is the most serious and the resistance to elastic deformation and failure is the weakest under this condition. The Brazilian splitting modulus decreases by 12% when deviatoric stress increases from 15 MPa to 20 MPa when the temperature is 100 °C. Accordingly, with the change of external temperature and pressure, the Brazilian splitting modulus of granite will increase, and appropriate temperature and pressure can improve the ability of rock to resist elastic deformation.

### 5. Modification of Granite MMTS Criterion Considering Different Occurrence Depths

In Section 4, the fracture toughness and tensile strength of granite affected by different occurrence depths are obtained. We substituted these parameters into the theoretical formula in Section 2 to study the accuracy of MMTS in predicting rock fracture characteristics.

#### 5.1. Comparative Analysis of Experimental Results and MMTS Criterion Prediction Results

When Equation (7) is combined with the calculation formulas of  $K_I$  and  $K_{II}$ , the following formula can be obtained:

$$\frac{K_{IC}}{K_I} = \cos^2 \theta_0 \left( \cos \theta_0 - 3 \frac{Y_I}{Y_{II}} \sin \frac{\theta_0}{2} \right) + \frac{1}{Y_I} \sqrt{\frac{2\pi r_c}{a}} T * \sin^2 \theta_0 \quad (11)$$

$$\frac{K_{IC}}{K_{II}} = \cos^2 \theta_0 \left( \frac{Y_I}{Y_{II}} \cos \theta_0 - 3 \sin \frac{\theta_0}{2} \right) + \frac{1}{Y_{II}} \sqrt{\frac{2\pi r_c}{a}} T * \sin^2 \theta_0 \quad (12)$$

According to Equations (11) and (12), a relationship between  $K_I/K_{IC}$  and  $K_{II}/K_{IC}$  can be established, and the fracture envelope under different temperatures and pressures can be obtained, as shown in Figure 5. As can be seen from Figure 5, with the rise in temperature and deviatoric stress, the fracture envelope shows obvious change characteristics, which indicates that various temperatures and pressures have different effects on the fracture mechanical properties of rocks.

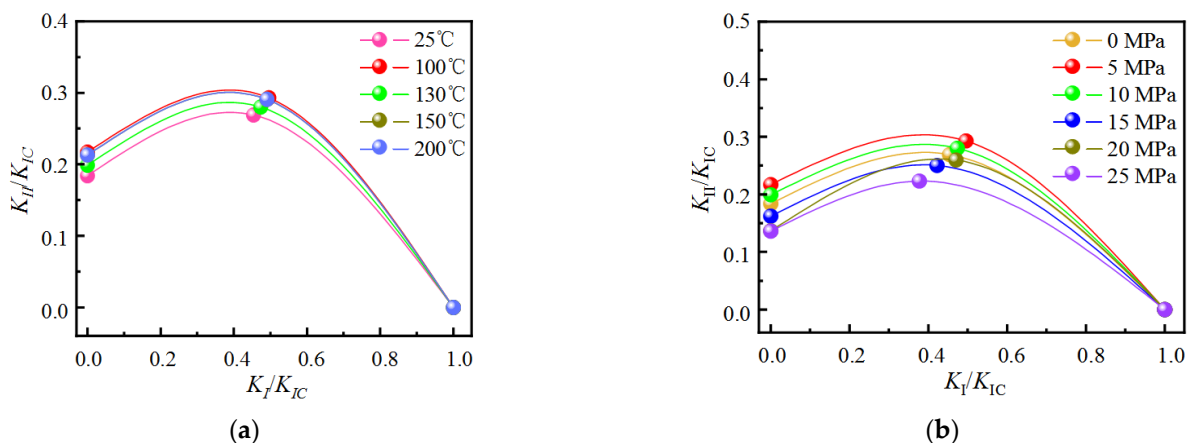


**Figure 5.** Fracture envelope under different conditions. (a) Fracture envelope at different temperatures; (b) Fracture envelope under different deviatoric stresses.

By combining Equations (9) and (10), the relationship between the mixed-mode parameter  $M^e$  and  $K_{eff}/K_{IC}$  is established. Figure 6 shows the comparison between the fitted curves of  $K_{eff}/K_{IC}$  and the predicted values of the traditional MTS theory and MMTS theory under various temperatures and pressures.

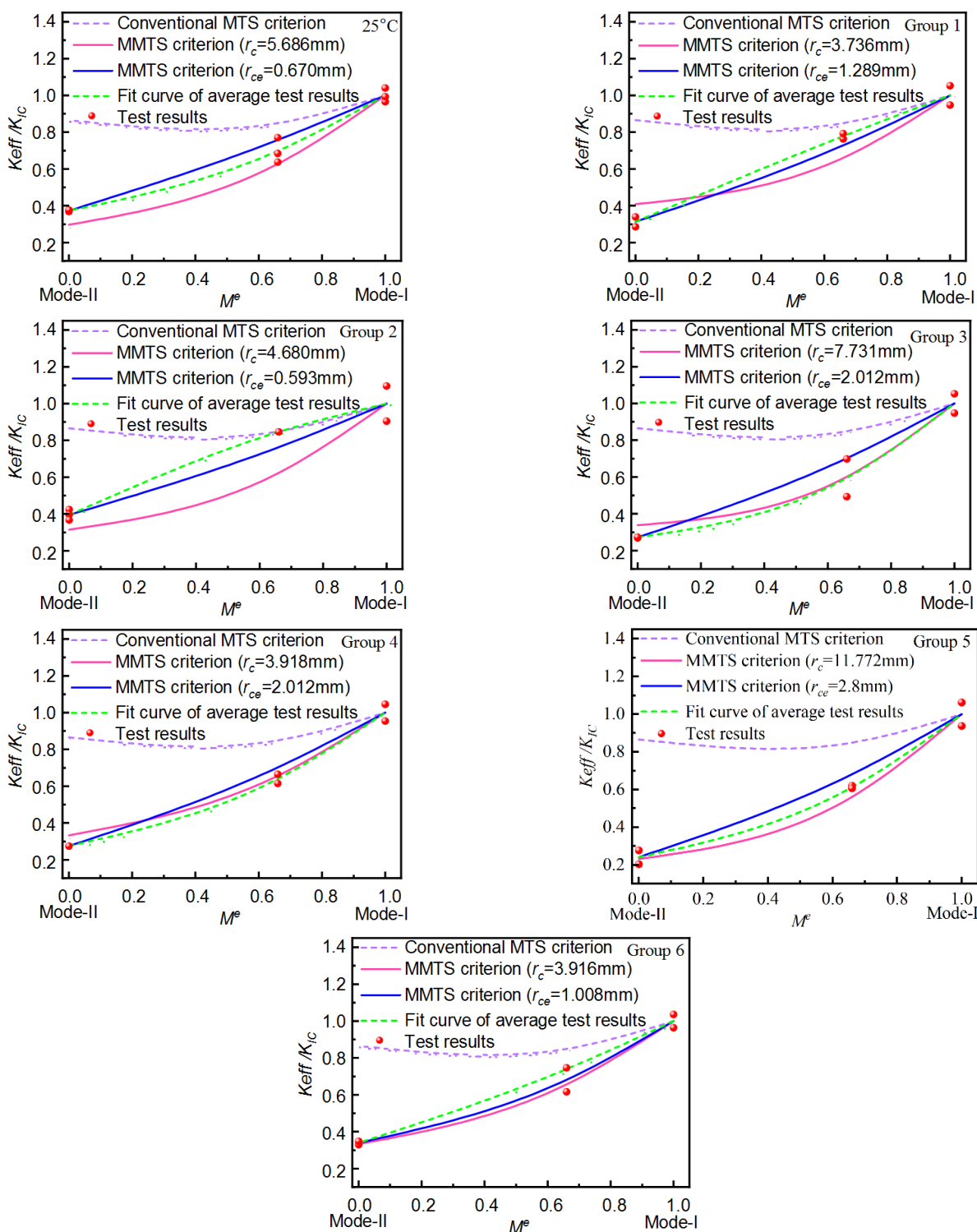


**Figure 6.** Comparison of the  $K_{eff}/K_{IC}$  ratio of granite SCB specimens with the theoretical value predicted by MMTS criterion.

It can be seen from Figure 6 that the theoretical prediction curve of the traditional MTS criterion deviates greatly from the test results, which may be mainly because the influence of  $T$ -stress is ignored. However, under different temperatures and pressures, the prediction curve of MMTS criterion after considering  $T$ -stress deviates greatly from the fitting curve of the average value of test results, and there is a large deviation from the experimental results. This indicates that the prediction of the Mode II fracture toughness

and mixed-mode (I+II) fracture toughness of granites with different occurrence depths by MMTS has bigger differences than the actual results. Next, the critical crack propagation radius will be deduced from the experimental results to better match the actual results of Mode II and mixed-mode (I+II) fracture toughness of granite. In addition, it is worth noting that the fracture envelope at different occurrence depths is distinguished, which indicates that the influence of various occurrence depths should be considered when predicting rock fracture toughness by fracture criteria.

### 5.2. The Modified MMTS Criteria

It can be seen from the analysis in Section 2 that the crack propagation radius,  $r_c$ , and fracture initiation angle,  $\theta_0$ , seriously affect the accuracy of MMTS criterion prediction. The modified critical crack propagation radius was defined as  $r_{ce}$ . By substituting the experimental results,  $K_{eff}/K_{IC}$ , into Equation (9), Equations (3) and (9) are simultaneously established to obtain the critical crack propagation radius,  $r_{ce}$ , which is in line with the actual experimental situation. By substituting  $r_{ce}$  into Equations (3) and (9), the modified MMTS prediction,  $K_{eff}/K_{IC}$ , curve is drawn, as shown by the solid blue line in Figure 6. It can be seen from Figure 6 that the MMTS prediction curve obtained by direct reverse calculation through experimental testing is in high agreement with the test results. This indicates that, compared with the  $r_c$  calculated by Equation (4),  $r_{ce}$  can better reflect the size of FPZ of granite samples with different occurrence depths. It can also be seen that the previous method of estimating the critical crack propagation radius directly by Equation (4) is not consistent with the actual situation. Maybe the fracture criterion needs to be further refined. Under the current MMTS theory, a new method for estimating or testing the critical crack propagation radius should be explored, or the  $r_c$  estimated by the previous method should be modified.  $r_{ce}/r_c$  is defined as the correction coefficient of crack propagation radius, which is expressed as  $\gamma$ . The changes of  $r_c$ ,  $r_{ce}$ , and  $\gamma(r_{ce}/r_c)$  with temperature and deviatoric stress were plotted, as shown in Figure 7.

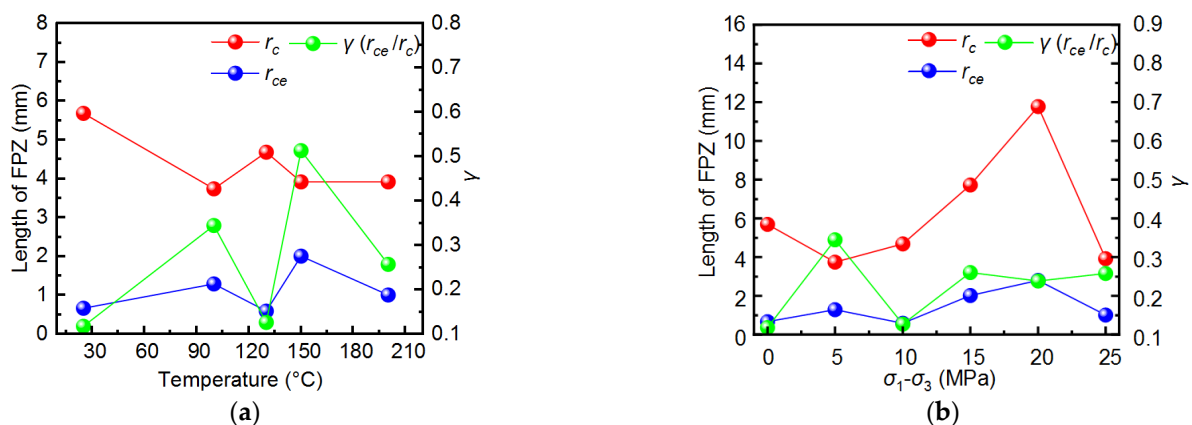


**Figure 7.** Changes of  $r_c$ ,  $r_{ce}$ , and  $\gamma(r_{ce}/r_c)$ . (a) Variation of  $r_c$ ,  $r_{ce}$ , and  $\gamma(r_{ce}/r_c)$  with temperature. (b) Variation of  $r_c$ ,  $r_{ce}$ , and  $\gamma(r_{ce}/r_c)$  with deviatoric stress.

As can be seen from Figure 7, there are great differences in  $r_c$  and  $r_{ce}$  values; under different heat treatment conditions,  $r_{ce}$  is smaller than  $r_c$ . With the increase in temperature and deviatoric stress, the changes of  $r_c$  and  $r_{ce}$  are not coordinated, and  $\gamma(r_{ce}/r_c)$  shows an upward trend, ranging from 0.118 to 0.514. This indicates that the critical crack propagation radius,  $r_c$ , obtained by Equation (4) cannot accurately reflect the size of FPZ. According to Section 4.1, the test results of fracture toughness under different heat treatment conditions and different modes have obvious differences. Therefore,  $r_c$  seriously affects the accuracy of MMTS criterion in predicting rock fracture toughness.

## 6. Numerical Simulation of Fracture of Granite Specimen

It can be seen from Section 5 that FPZ size affects the accuracy of MMTS criterion in predicting the fracture mechanical behavior of granite with different occurrence depths. In order to verify that FPZ is a critical reason for the accuracy of MMTS criterion in predicting granite fracture trajectory, we used ABAQUS numerical software and, based on the extended finite element method (XFEM), conducted numerical simulations for specimens with different occurrence depths and different crack inclination angles. The model was set as a two-dimensional plane stress model, and the maximum principal stress and damage variable were selected as the criterion for crack initiation and propagation [51]. Due to space limitation, Figure 8 shows the numerical simulation results with typical  $r_{ce}$  data.

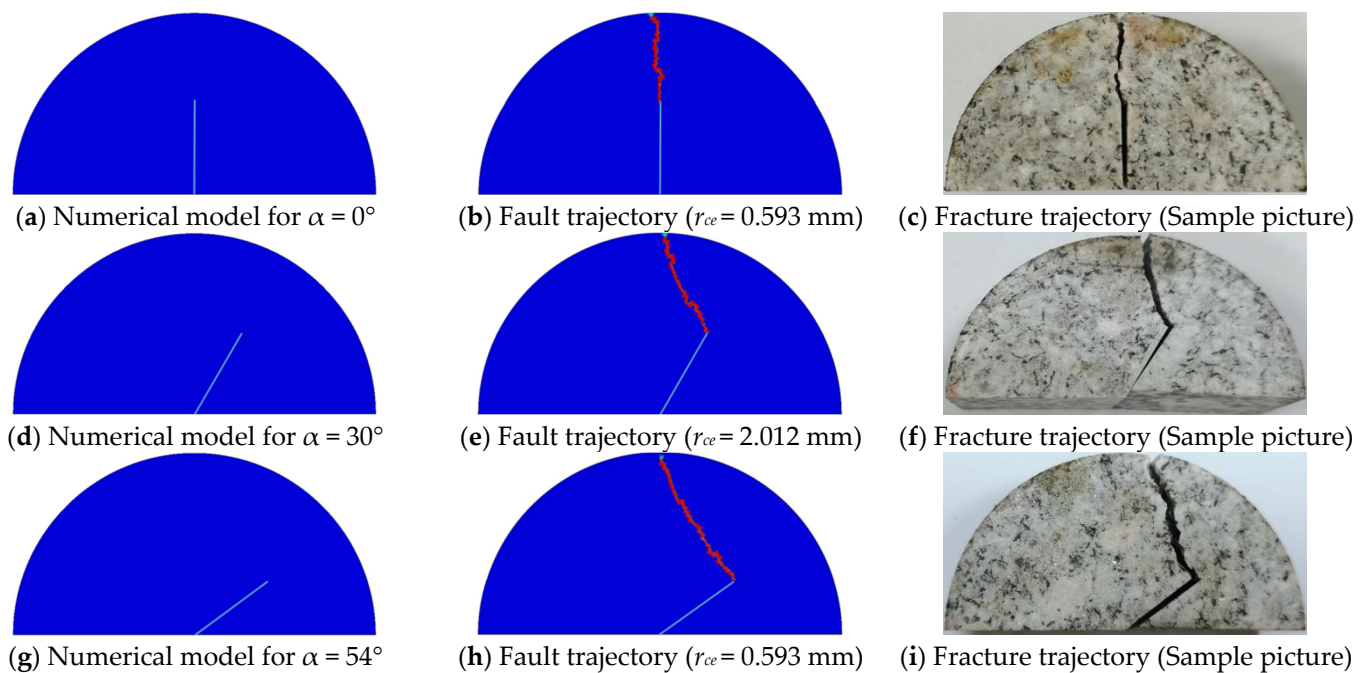


**Figure 8.** Comparison between the results of granite fracture trajectories after correction of critical crack propagation radius and the experimental results.

It can be seen from Figure 8 that the crack expands along the crack tip and the loading point in the simulation results, and the crack initiation angle increases with the increase in the prefabricated crack angle, which is consistent with the test results. The results of granite crack growth trajectory obtained using the modified critical crack growth radius,  $r_{ce}$ , are in good agreement with the experimental results. The numerical simulation results show that temperature and three-dimensional pressure affect the fracture trajectory of granite by influencing FPZ, which is an important factor affecting the prediction accuracy of MMTS criterion. Therefore, it is crucial to accurately find the critical crack propagation radius for accurately predicting the Mode II fracture toughness, mixed-mode (I+II) fracture toughness, and fracture trajectory of granite with different occurrence depths.

## 7. Discussion

The temperature and geostress of geothermal reservoirs with different occurrence depths vary, and the mechanical properties of rock are different. Temperature and pressure do not affect rocks in the same way. As the rock is composed of multiple mineral components and the mineral particles have different thermal expansion coefficients, the thermal expansion between mineral particles is not coordinated in the process of heating and insulation, resulting in thermal stress among mineral particles. When the thermal stress is large enough, it can promote the expansion of the primary cracks and produce

microcracks [52–54], weakening the mechanical properties of the rock. In addition, the water inside the rock evaporates during the heating process, producing more micropores, reducing the compactness of the rock, thereby weakening the mechanical properties of the rock. On the contrary, the appropriate pressure can facilitate pore closure, suppress the propagation of primary fractures and new fractures of the rock, weaken the thermal expansion of the rock, make the rock denser, and further improve the mechanical properties of the rock [55,56]. Therefore, due to the different dominant positions of temperature and pressure, the mechanical properties of rocks will increase or decrease.

The experimental results show that under different temperature pressure coupling mechanisms, the fracture toughness, Brazilian splitting strength, and Brazilian splitting modulus of rock fluctuate up and down with the increase in confining pressure and temperature, showing obvious nonlinear characteristics. For example, when the temperature is 100 °C, the axial pressure is 25 MPa, and the lateral pressure is 20 MPa, the mixed-mode (I+II) fracture toughness, Brazilian splitting strength, and the Brazilian splitting modulus of the rock are higher than those at room temperature. Meng et al. [57] conducted triaxial compression tests on limestone under high temperature. The results showed that the peak stress of rock increased with the increase in confining pressure from 0 MPa to 30 MPa at a certain temperature. Funatsu et al. [58] tested the fracture toughness of Kimachi sandstone under the coupling of temperature and pressure. The results show that the effective fracture toughness increases with the increase in confining pressure from 1 MPa to 5 MPa when the temperature is constant. The above research results show that appropriate pressure can counteract the deterioration of rock mechanical properties caused by temperature and improve the mechanical properties of rock. When the temperature is 100 °C, the axial pressure is 60 MPa, and the lateral pressure is 40 MPa, the mixed-mode (I+II) fracture toughness, Brazilian splitting strength, and Brazilian splitting modulus of the rock are lower than those at room temperature. This may be due to the severe crystal deformation and slip in the rock caused by excessive three-dimensional pressure, and the internal fracture is more serious, leading to the reduction of the mechanical properties of the rock. Based on the above analysis, it can be seen that under different occurrence depths, the ability of rock to resist tension, shear, and tension shear fracture is different.

The size of the fracture process zone (FPZ) is closely related to the internal microstructure of the rock. FPZ is not only formed in homogeneous and dense media, but also under temperature and pressure damage, its original state should contain some pores and cracks. It is known from the test results that under the action of temperature and three-dimensional pressure, the crack growth radius before and after correction fluctuates and decreases with the increase in temperature. Meng et al. [47] carried out fracture mechanics experiments under different temperatures and found that FPZ value gradually increases with the increase in temperature. There are significant differences compared with this research. This is mainly because, under the combined action of temperature and pressure, complex physical and chemical reactions occur in the rock. In addition to the role of thermal stress, three-dimensional pressure can promote the closure of pores and fractures in the rock and inhibit the initiation and propagation of microcracks, and the FPZ value of granite will also be affected.

The modified MMTS criterion can accurately predict the fracture characteristics of geothermal reservoirs with different occurrence depths. According to Equations (3)–(9), the crack growth radius is closely related to the crack growth angle, mixed-mode (I+II), and Mode-II fracture toughness parameters, and affects the macro fracture characteristics. It can be seen from Section 5 that the modified crack growth radius ( $r_{ce}$ ) can accurately predict the fracture toughness of rock compared with  $r_c$ . This shows that  $r_{ce}$  can better reflect the FPZ size of rock. In addition, some scholars [21,22,47,59] also pointed out that the actual FPZ size calculated by Equation (4) was inconsistent. Therefore, it is necessary to correct  $r_c$  when predicting the fracture characteristics of geothermal reservoirs with different depths.



## 8. Conclusions

In this paper, the accuracy of MMTS in predicting the fracture mechanical behavior of geothermal reservoirs is analyzed. Firstly, the theoretical formula is derived, and then the MMTS criterion is analyzed and modified by heat treatment, three-point bending fracture, and Brazilian splitting tests of granite samples in a geothermal reservoir under different temperatures and three-dimensional pressures. The main research conclusions are as follows:

- (1) FPZ seriously affects fracture initiation angle and mixed-mode (I+II) fracture toughness, which affects the accuracy of MMTS in predicting rock fracture behavior. Considering the influence of different occurrence depths,  $r_c$  fails to accurately reflect the actual size of FPZ, so it needs to be modified to obtain results consistent with the actual. The Mode II fracture toughness and mixed-mode (I+II) fracture toughness of granites with different occurrence depths predicted by MMTS are significantly different from the measured values.
- (2) The  $r_{ce}$  obtained from the reverse solution of the test results is smaller than the  $r_c$ . With the increase in temperature and deviatoric stress, the changes of  $r_c$  and  $r_{ce}$  are not coordinated. When the  $r_{ce}$  obtained by the reverse calculation of the experimental data is substituted into the MMTS criterion, the predicted results are in good agreement with the experimental results. Temperature and three-dimensional stress affect the size of FPZ by changing the microscopic properties of rock. It is also verified by numerical simulation that after correcting the critical crack propagation radius, the fracture trajectories obtained are basically consistent with the experimental results. Further theoretical and experimental studies are needed to evaluate the fracture characteristics of geothermal reservoirs at different depths predicted by MMTS criteria.
- (3) Under the influence of temperature and pressure, the Brazilian splitting strength,  $\sigma_t$ , of granite fluctuates and rises with the increase in temperature. With the increase in deviatoric stress, Brazilian splitting strength and Brazilian splitting modulus first increase, then decrease, and then increase.

**Author Contributions:** Conceptualization, C.L. (Chenbo Liu) and G.F.; data curation, Z.D. and G.L.; formal analysis, J.W. and Y.T.; funding acquisition, G.F.; methodology, C.L. (Chenbo Liu) and G.F.; resources, H.X. (Hongqiang Xie), H.X. (Huining Xu), Y.H. (Yaoqing Hu), C.L. (Chun Li) and Y.H.; writing—review and editing, C.L. (Chenbo Liu), G.F., G.L., Y.H. (Yaoqing Hu), Y.H. (Yuefei Hu), Q.W. and L.C. All authors have read and agreed to the published version of the manuscript.

**Funding:** This study was funded by the National Natural Science Foundation of China (No. 52104143), the open fund of Key Laboratory of Deep Earth Science and Engineering (Sichuan University), Ministry of Education (Grant No. DESE202104), the Natural Science Foundation of Sichuan Province, China (Grant No. 52104143), the Fundamental Research Funds for the Central Universities (No. 2021SCU12039), the College Students' Innovative Entrepreneurial Training Plan Program (No. 20220708L), and China Postdoctoral Science Foundation (Grant No. 2020M673225). These supports are gratefully acknowledged.

**Institutional Review Board Statement:** Not applicable.

**Informed Consent Statement:** Not applicable.

**Data Availability Statement:** The data that support the findings of this study are available from the corresponding author upon reasonable request.

**Conflicts of Interest:** No conflict of interest exists in the submission of this manuscript.

## References

1. Xie, H.; Li, C.; Zhao, T.; Chen, J.; Liao, J.; Ma, J.; Li, B. Conceptualization and evaluation of the exploration and utilization of low/medium-temperature geothermal energy: A case study of the Guangdong-Hong Kong-Macao Greater Bay Area. *Geomech. Geophys. Geo-Energy Geo-Resour.* **2020**, *6*, 18. [[CrossRef](#)]
2. Sun, Z.; Zhang, X.; Xu, Y.; Yao, J.; Wang, H.; Lv, S.; Sun, Z.; Huang, Y.; Cai, M.; Huang, X. Numerical simulation of the heat extraction in EGS with thermal hydraulic-mechanical coupling method based on discrete fractures. *Energy* **2017**, *120*, 20–33. [[CrossRef](#)]
3. Ye, Z.; Wang, J.; Hu, B. Comparative study on heat extraction performance of geothermal reservoirs with presupposed shapes and permeability heterogeneity in the stimulated reservoir volume. *J. Pet. Sci. Eng.* **2021**, *206*, 109023. [[CrossRef](#)]
4. Liu, B.; Suzuki, A.; Watanabe, N.; Ishibashi, T.; Sakaguchi, K.; Ito, T. Fracturing of granite rock with supercritical water for superhot geothermal resources. *Renew. Energy* **2022**, *184*, 56–67. [[CrossRef](#)]
5. Wang, G.; Zhang, W.; Ma, F.; Lin, W.; Liang, J.; Zhu, X. Overview on hydrothermal and hot dry rock researches in China. *China Geol.* **2018**, *1*, 273–285. [[CrossRef](#)]
6. Zhu, J.; Hu, K.; Lu, X.; Huang, X.; Liu, K.; Wu, X. A review of geothermal energy resources, development, and applications in China: Current status and prospects. *Energy* **2015**, *93*, 466–483. [[CrossRef](#)]
7. Ganguly, S.; Kumar, M.S.M. Geothermal reservoirs—A brief review. *J. Geol. Soc. India* **2012**, *79*, 589–602. [[CrossRef](#)]
8. Zhou, Z.; Jin, Y.; Zeng, Y.; Zhang, X.; Zhou, J.; Zhuang, L.; Xin, S. Investigation on fracture creation in hot dry rock geothermal formations of China during hydraulic fracturing. *Renew. Energy* **2020**, *153*, 301–303. [[CrossRef](#)]
9. Lu, S.M. A global review of enhanced geothermal system (EGS). *Renew. Sustain. Energy Rev.* **2018**, *81*, 2902–2921. [[CrossRef](#)]
10. Zhang, Y.; Zhao, G. A global review of deep geothermal energy exploration: From a view of rock mechanics and engineering. *Geomech. Geophys. Geo-Energy Geo-Resour.* **2019**, *6*, 4. [[CrossRef](#)]
11. Kang, F.; Tang, C.; Li, Y.; Li, T.; Men, J. Challenges and opportunities of enhanced geothermal systems: A review. *Chin. J. Eng.* **2022**, *44*, 1767–1777. (In Chinese)
12. Olasolo, P.; Juarez, M.C.; Morales, M.P.; D’Amico, S.; Liarte, I.A. Enhanced geothermal systems (EGS): A review. *Renew. Sustain. Energy Rev.* **2016**, *56*, 133–144. [[CrossRef](#)]
13. Richards, H.G.; Parker, R.H.; Green, A.S.P.; Jones, R.H.; Nicholls, J.D.M.; Nicol, D.A.C.; Randall, M.M.; Richards, S.; Stewart, R.C.; Willisrichards, J. The performance and characteristics of the experimental hot dry rock geothermal reservoir at rosemanowes, cornwall (1985–1988). *Geothermics* **1994**, *23*, 73–109. [[CrossRef](#)]
14. Seibt, P.; Hoth, P. The neustadt-glewe geothermal station: From surveys to active operation. *Therm. Eng.* **2004**, *51*, 494–497.
15. Schill, E.; Genter, A.; Cuenot, N.; Kohl, T. Hydraulic performance history at the Soultz EGS reservoirs from stimulation and long-term circulation tests. *Geothermics* **2017**, *70*, 110–124. [[CrossRef](#)]
16. Ayatollahi, M.R.; Sistaninia, M. Mode-II fracture study of rocks using Brazilian disk specimens. *Int. J. Rock Mech. Min. Sci.* **2011**, *48*, 819–826. [[CrossRef](#)]
17. Akbardoost, J.; Ayatollahi, M.R. Experimental analysis of mixed mode crack propagation in brittle rocks: The effect of non-singular terms. *Eng. Fract. Mech.* **2014**, *129*, 77–89. [[CrossRef](#)]
18. Yang, J.; Liang, W.; Chen, Y.; Li, L.; Lian, H. Experiment research on the fracturing characteristics of mudstone with different degrees of water damage. *Chin. J. Rock. Mech. Eng.* **2017**, *36*, 2431–2440. (In Chinese)
19. Wang, C.; Wang, S. Modified generalized maximum tangential stress criterion for simulation of crack propagation and its application in discontinuous deformation analysis. *Eng. Fract. Mech.* **2022**, *259*, 108159. [[CrossRef](#)]
20. Aliha, M.R.M.; Samareh-Mousavi, S.S.; Mirsayar, M.M. Loading rate effect on mixed mode I/II brittle fracture behavior of PMMA using inclined cracked SBB specimen. *Int. J. Solids Struct.* **2021**, *232*, 111177. [[CrossRef](#)]
21. Feng, G.; Wang, X.; Kang, Y.; Zhang, Z. Effect of thermal cycling-dependent cracks on physical and mechanical properties of granite for enhanced geothermal system. *Int. J. Rock Mech. Min.* **2020**, *134*, 104476. [[CrossRef](#)]
22. Feng, G.; Wang, X.; Wang, M.; Kang, Y. Experimental investigation of thermal cycling effect on fracture characteristics of granite in a geothermal-energy reservoir. *Eng. Fract. Mech.* **2020**, *235*, 107180. [[CrossRef](#)]
23. Tang, S. The effect of T-stress on the fracture of brittle rock under compression. *Int. J. Rock Mech. Min.* **2015**, *79*, 86–98. [[CrossRef](#)]
24. Tang, S.; Bao, C.; Liu, H. Brittle fracture of rock under combined tensile and compressive loading conditions. *Can. Geotech. J.* **2017**, *54*, 88–101. [[CrossRef](#)]
25. Tang, S.; Zhang, H. The characteristics of crack initiation at the crack tip in rock material. *Chin. J. Rock. Mech. Eng.* **2017**, *36*, 552–561. (In Chinese)
26. Wu, S.; Li, L.; Zhang, X. *Rock Mechanics*; Higher Educational Press: Beijing, China, 2021; pp. 28–29.
27. Ma, F.; Liu, G.; Zhao, Z.; Xu, H.; Wang, G. Coupled Thermo-Hydro-Mechanical Modeling on the Rongcheng Geothermal Field, China. *Rock Mech. Rock Eng.* **2022**, *55*, 5209–5233. [[CrossRef](#)]
28. Li, T.; Tang, C.; Rutqvist, J.; Hu, M. TOUGH-RFPA: Coupled thermal-hydraulic-mechanical Rock Failure Process Analysis with application to deep geothermal wells. *Int. J. Rock Mech. Min.* **2021**, *142*, 104726. [[CrossRef](#)]

29. Wang, K.; Liu, Z.; Zeng, T.; Wang, F.; Shen, W.; Shao, J. Performance of enhanced geothermal system with varying injection-production parameters and reservoir properties. *Appl. Therm. Eng.* **2022**, *207*, 118160. [[CrossRef](#)]
30. Zhang, X.; Kong, B.; Yu, S.; Zhai, J.; Zhang, W.; Wang, R. Time series characteristics and difference analysis of AE of coal deformation and fracture under different damage and failure conditions. In Proceedings of the Third International Conference on Optoelectronic Science and Materials (ICOSM 2021), Hefei, China, 10–12 September 2021.
31. Zhang, C.; Yu, B.; Feng, Y.; Yuan, J.; Deng, J. Integrated Approach for the Wellbore Instability Analysis of a High-pressure, High-temperature Field in the South China Sea. In Proceedings of the IOP Conference Series: Earth and Environmental Science, Beijing, China, 23–26 October 2020.
32. Wang, C.; Liu, Z.; Zhou, H.; Wang, K.; Shen, W. A novel true triaxial test device with a high-temperature module for thermal-mechanical property characterization of hard rocks. *Eur. J. Environ. Civ. Eng.* **2022**. [[CrossRef](#)]
33. Guo, T.; Tang, S.; Liu, S.; Liu, X.; Zhang, W.; Qu, G. Numerical simulation of hydraulic fracturing of hot dry rock under thermal stress. *Eng. Fract. Mech.* **2021**, *240*, 107350. [[CrossRef](#)]
34. Kumari, W.G.P.; Ranjith, P.G.; Perera, M.S.A.; Li, X.; Li, L.H.; Chen, B.K.; Avanthi Isaka, B.L.; De Silva, V.R.S. Hydraulic fracturing under high temperature and pressure conditions with micro CT applications: Geothermal energy from hot dry rocks. *Fuel* **2018**, *230*, 138–154. [[CrossRef](#)]
35. Meng, Q.; Liu, J.; Pu, H.; Yu, L.; Wu, J.; Wang, C. Mechanical properties of limestone after high-temperature treatment under triaxial cyclic loading and unloading conditions. *Rock Mech. Rock Eng.* **2021**, *54*, 6413–6437. [[CrossRef](#)]
36. Ding, K.; Wang, L.; Ren, B.; Li, Z.; Wang, S.; Jiang, C. Experimental study on relative permeability characteristics for CO<sub>2</sub> in sandstone under high temperature and overburden pressure. *Minerals* **2021**, *11*, 956. [[CrossRef](#)]
37. Ergodan, F.; Sih, G.C. On the crack extension in plates under plane loading and transverse shear. *J. Basic Eng.* **1963**, *85*, 519–525.
38. Mirsayar, M.M.; Razmi, A.; Aliha, M.R.M.; Berto, F. Frictional crack initiation and propagation in rocks in rock materials. *Eng. Fract. Mech.* **2018**, *190*, 186–197. [[CrossRef](#)]
39. Williams, M.L. On the stress distribution at the base of a stationary crack. *ASME. J. Appl. Mech.* **1957**, *24*, 109–114. [[CrossRef](#)]
40. Saghafi, H.; Ayatollahi, M.R.; Sistaninia, M. A modified MTS criterion (MMTS) for mixed-mode fracture toughness assessment of brittle materials. *Mater. Sci. Eng. A-Struct. Mater. Prop. Microstruct. Process.* **2010**, *527*, 5624–5630. [[CrossRef](#)]
41. Ayatollahi, M.R.; Aliha, M.R.M. Wide range data for crack tip parameters in two disc-type specimens under Mixed-mode loading. *Comput. Mater. Sci.* **2017**, *38*, 660–670. [[CrossRef](#)]
42. Yang, J.; Lian, H.; Liang, W.; Nguyen, V.P.; Chen, Y. Experimental investigation of the effects of supercritical carbon dioxide on fracture toughness of bituminous coals. *Int. J. Rock Mech. Min.* **2018**, *107*, 233–242. [[CrossRef](#)]
43. Wei, M.; Dai, F.; Xu, N.; Liu, Y.; Zhao, T. Fracture prediction of rocks under mode I and mode II loading using the generalized maximum tangential strain criterion. *Eng. Fract. Mech.* **2017**, *186*, 21–38. [[CrossRef](#)]
44. Aliha, M.R.M.; Ayatollahi, M.R. Two-parameter fracture analysis of SCB rock specimen under mixed mode loading. *Eng. Fract. Mech.* **2013**, *103*, 115–123. [[CrossRef](#)]
45. Schmidt, R.A. A microcrack model and its significance to hydraulic fracturing and fracture toughness testing. In Proceedings of the 21st US Rock Mechanics Symposium, Rolla, MI, USA, 27–30 May 1980; pp. 581–590.
46. Alneasan, M.; Behnia, M.; Bagherpour, R. Frictional crack initiation and propagation in rocks under compressive loading. *Theor. Appl. Fract. Mech.* **2018**, *97*, 189–203. [[CrossRef](#)]
47. Meng, T.; Xue, G.; Ma, J.; Yang, Y.; Liu, W.; Zhang, J.; Jiao, B.; Fang, S.; Ren, G. Mixed mode fracture tests and inversion of FPZ at crack tip of overlying strata in underground coal gasification combustion cavity under real-time high temperature condition. *Eng. Fract. Mech.* **2020**, *239*, 107298. [[CrossRef](#)]
48. Feng, G.; Liu, C.; Wang, J.; Tao, Y.; Duan, Z.; Xiang, W. Experimental study on the fracture toughness of granite affected by coupled mechanical-thermo. *Lithosphere* **2022**, *2022*, 5715093. [[CrossRef](#)]
49. Kuruppu, M.D.; Obara, Y.; Ayatollahi, M.R.; Chong, K.P.; Funatsu, T. ISRM suggested method for determining the Mode I fracture toughness using semi-circular bend specimen. *Rock Mech. Rock Eng.* **2014**, *47*, 267–274. [[CrossRef](#)]
50. Sun, Z.; Feng, G.; Song, X.; Meng, T.; Zhu, D.; Zhai, Y.; Wang, Z. Effects of CO<sub>2</sub> state and anisotropy on the progressive failure characteristics of bituminous coal: An experimental study. *Chin. J. Rock. Mech. Eng.* **2022**, *41*, 70–81. (In Chinese)
51. Suo, Y.; Chen, Z.; Rahman, S.S.; Song, H. Experimental and numerical investigation of the effect of bedding layer orientation on fracture toughness of shale rocks. *Rock Mech. Rock Eng.* **2020**, *53*, 3625–3635. [[CrossRef](#)]
52. Meng, F.; Song, J.; Wong, L.N.Y.; Wang, Z.; Zhang, C. Characterization of roughness and shear behavior of thermally treated granite fractures. *Eng. Geol.* **2021**, *293*, 106287. [[CrossRef](#)]
53. Zhao, F.; Sun, Q.; Zhang, W. Environ. Fractal analysis of pore structure of granite after variable thermal cycles. *Earth Sci.* **2019**, *78*, 677. [[CrossRef](#)]
54. Xiao, W.; Yu, G.; Li, H.; Zhang, D.; Li, S.; Yu, B. Thermal cracking characteristics and mechanism of sandstone after high-temperature treatment. *Fatigue Fract. Eng. Mater. Struct.* **2021**, *44*, 3169–3185. [[CrossRef](#)]
55. Taheri, A.; Zhang, Y.; Munoz, H. Performance of rock crack stress thresholds determination criteria and investigating strength and confining pressure effects. *Constr. Build. Mater.* **2020**, *243*, 118263. [[CrossRef](#)]
56. Feng, G.; Kang, Y.; Chen, F.; Liu, Y.; Wang, X. The influence of temperatures on mixed-mode (I plus II) and mode-II fracture toughness of sandstone. *Eng. Fract. Mech.* **2018**, *189*, 51–63. [[CrossRef](#)]

- 
57. Meng, Q.; Qian, W.; Liu, J.; Zhang, M.; Lu, M.; Wu, Y. Analysis of triaxial compression deformation and strength characteristics of limestone after high temperature. *Arab. J. Geosci.* **2020**, *13*, 153. [[CrossRef](#)]
  58. Funatsu, T.; Kuruppu, M.; Matsui, K. Effects of temperature and confining pressure on mixed-mode (I-II) and mode-II fracture toughness of Kimachi sandstone. *Int. J. Rock Mech. Min.* **2014**, *67*, 1–8. [[CrossRef](#)]
  59. Li, Y.; Dai, F.; Wei, M.; Du, H. Numerical investigation on dynamic fracture behavior of cracked rocks under mixed mode I/II loading. *Eng. Fract. Mech.* **2020**, *235*, 107176. [[CrossRef](#)]